Electrochemical Growth of Epitaxial Eosin/ZnO Hybrid Films

T. Pauporté,*,† T. Yoshida,‡ R. Cortès,§ M. Froment,§ and D. Lincot†

Laboratoire d'Electrochimie et Chimie Analytique, UMR−CNRS 7575, École Nationale Supérieure de Chimie de Paris, 11 rue P. et M. Curie, 75231 Paris Cedex 05, France, Environmental and Renewable Energy Systems, Graduate School of Engineering, Gifu University, Yanagido 1-1, Gifu 501-1193, Japan, and Physique des Liquides et Electrochimie, UPR 15 CNRS, Conventionné avec l'Université P. et M. Curie, 75252 Paris Cedex 0.5, France

Received: January 13, 2003; In Final Form: April 16, 2003

ZnO-based organic/inorganic hybrid semiconductor compounds have been grown heteroepitaxially in one step at low temperature by a simple electrochemical method from an oxygenated zinc chloride aqueous solution. The substrate is GaN(0001) single crystals, and the organic compound is a dye, eosin Y, dissolved in the deposition bath. The epitaxial growth of the hybrid is observed between −1.2 and −1.5 V versus the mercurous sulfate electrode. The deposit morphology changes dramatically with the deposition potential in relation to the redox state of eosin Y during the deposition. Various experiments show that an open nanostructured film is formed when the dye is co-deposited in its reduced form, while a compact structure is formed when the dye is included in its oxidized form. The structural relationship with single crystalline GaN and the quality of epitaxial ZnO have been studied by reflection high-energy electron diffraction (RHEED) and five-circle X-ray diffraction techniques. The polycrystalline phase content is negligible. The in-plane misorientation increases significantly with the dye loading, that is, with negative potential. This is interpreted in terms of detrimental effect of the presence of dye on the ZnO structural unit matching with the GaN surface. The epitaxial nature of these hybrid organic/inorganic films opens new perspectives for high quality device applications.

1. Introduction

Mixing inorganic and organic compounds in an unique composite material has appeared for a long time as a simple way to combine specific properties brought separately by each component and is presently largely used for instance in the paint and polymer industries. More recently, the possibility of combining organic and inorganic components in a more intimate way by means of covalent or iono-covalent bonds has opened wide the application fields of inorganic−organic hybrid compounds (see ref 1 for a recent review and references therein). These strong interactions not only allow self-assembly processes but also new interesting properties can arise from the close interactions between both components.

Singular hybrid structures have been synthesized by means of wet mild chemistry methods such as sol−gel processing,[1,2] ion exchange,[3] use of Langmuir−Blodgett films,[4] or surface adsorption of organic molecules[5,6] and have been described during the past decade. For instance, the organic component can be entrapped in a nanostructured inorganic matrix or an organic−inorganic functional nanocluster can be bridged by organic connectors.[1] The occurrence of new properties is illustrated by the active layer of dye sensitized solar cells (DSSC), where the generated electron−hole pair in the dyes under illumination is separated thanks to intimate contact with the nanostructured large band gap semiconductor matrix.[5,7,8] For inorganic materials, such as semiconductors which are under focus in this paper, the growth of high quality compounds generally requires high-temperature processes (>300 °C) which are inconsistent with the lack of thermal stability of organic compounds. This difficulty is classically overcome in the case of DSSC by dip adsorption of the dye from a solution after annealing of the porous semiconductor film at high temperature. Unfortunately, this stepwise process is time-consuming and does not allow the use of organic substrates (for instance, flexible polymer substrates). Moreover, a final adsorption process is perhaps not the best way to promote strong intermolecular interactions between the components. It has been shown by one of us that metallo-organic[9,10] or organic[10−14] dyes/ZnO hybrid films can be one-step deposited at low temperature (70−80 °C) by cathodic electrodeposition. The ZnO matrix has been shown well-crystallized. Moreover, the organic/inorganic compound interactions lead to original ZnO film morphologies and nanostructures have been observed. Yoshida and co-workers have shown that the formation of the different dye/ZnO hybrids is due to dye anchoring on the inorganic compound by means of sulfonic,[9,10] carboxyl,[10−13] or phosphate[14] functions.

The single crystalline nature of the nanostructured semiconductor matrix is considered an important objective to achieve high efficiency devices since it allows avoiding electrical losses related to the presence of grain boundaries. Epitaxial growth can be considered as the ultimate challenge since it provides in addition the best coherence with the substrate, allowing optimal charge transfer at the interface between the substrate and the hybrid structure. It also allows collective properties in the basal plane (i.e., photonic, laser properties), in the hybrid film, or between pillar or dots if the hybrid has a noncontinuous two-dimensional structure. The heteroepitaxial growth of ZnO has

* To whom correspondence should be addressed. E-mail: pauporte@ext.jussieu.fr.
† École nationale Supérieure de Chimie de Paris.
‡ Gifu University.
§ Conventionné avec l'Université P. et M. Curie.

10.1021/jp034079g CCC: $25.00
Published on Web 08/26/2003

been successfully achieved by electrochemistry.[15−17] These results were the basis of the challenging study to achieve epitaxial growth of dye/ZnO hybrids.

The electrochemical deposition method of ZnO consists of an electrochemically induced surface precipitation of zinc oxide by the production of an excess of OH^- species by reduction of an oxygen precursor (O_2,[15−19] NO_3^-,[20] H_2O_2[13,21,22]). Hydroxide ions under supersaturation react with Zn^{2+} dissolved ions to give ZnO ($Zn^{2+} + 2OH^- \rightarrow ZnO + H_2O$). The ZnO crystallographic orientation is governed by the single crystalline substrate when the lattice mismatch between both compounds is low.

In the present work, epitaxial hybrid films have been cathodically deposited in the presence of 21 μM eosin Y (EY) by reduction of dissolved O_2 oxygen precursor ($O_2 + 2H_2O + 4e^- \rightarrow 4OH^-$). The single crystalline substrates used, GaN-(0001), present a low mismatch with ZnO(0001), with $(a_{ZnO} - a_{GaN})/a_{GaN} = 2.4\%$.[23]

2. Experimental Section

The substrates were n-type GaN(0001) single crystalline layers deposited by metal−organic vapor-phase epitaxy (MOVPE) onto a sapphire(0001) single crystalline wafer. They presented a surface defect density of 1 μm^{-2}. The etching consisted of a treatment of 30 min in 28% NH_4OH at 50 °C.[17] The substrates were subsequently thoroughly rinsed with MilliQ quality water, dried under an argon stream, and mounted as an electrode. The electrical contact was taken on GaN by means of a Ga−In eutectic dot. The depositions were carried out at a controlled potential E_d during a period of time t_d in a classical three-electrode cell. They were performed with a PAR 273A potentiostat from EG&G. All the potentials are referred to the saturated mercurous sulfate electrode (MSE with a potential of +0.65 V versus NHE). The counter electrode was a platinum wire. The deposition bath temperature was set at 80 °C with a thermostat. The working electrode was fixed vertically, the deposition bath being stirred by a magnetic stirring bar at 100 rotations per minute. The electrolytic solution contained 5 mM reagent grade $ZnCl_2$ (Prolabo) and 0.1 M reagent grade KCl (Prolabo) as the supporting electrolyte. The EY concentration (21 μM) was adjusted by adding a small volume of a concentrated EY stock solution prepared from a sodium salt (85%, Kanto). An oxygen/argon gas mixture was bubbled in the deposition bath, and the oxygen concentration, fixed by the volumetric ratio between these two gases, is expressed as a percentage of the saturation concentration (8×10^{-4} M). The dye loading of the deposits was determined with films prepared onto F:SnO_2 coated glass substrate by following the procedure described in detail elsewhere.[12]

The morphology of the films was studied with a Stereoscan 440 scanning electron microscope from Leica. Cross sections of films deposited onto Si wafer/F:SnO_2 were prepared by mechanical grinding and ion milling. They were observed by transmission electron microscopy (JEOL 100CX2 100 keV). The epitaxial growth was studied by reflection high-energy electron diffraction (RHEED) observations. A quantitative determination of the structure and the epitaxial orientation of the film was achieved by X-ray diffraction method, using a five-circle goniometer with a Cu Kα source especially designed for a thin film study.[24] In this device, the incident beam is at a glancing angle (0.6°) and the detector is positioned at a 2θ angle corresponding to a Bragg diffraction angle characteristic of the deposit.

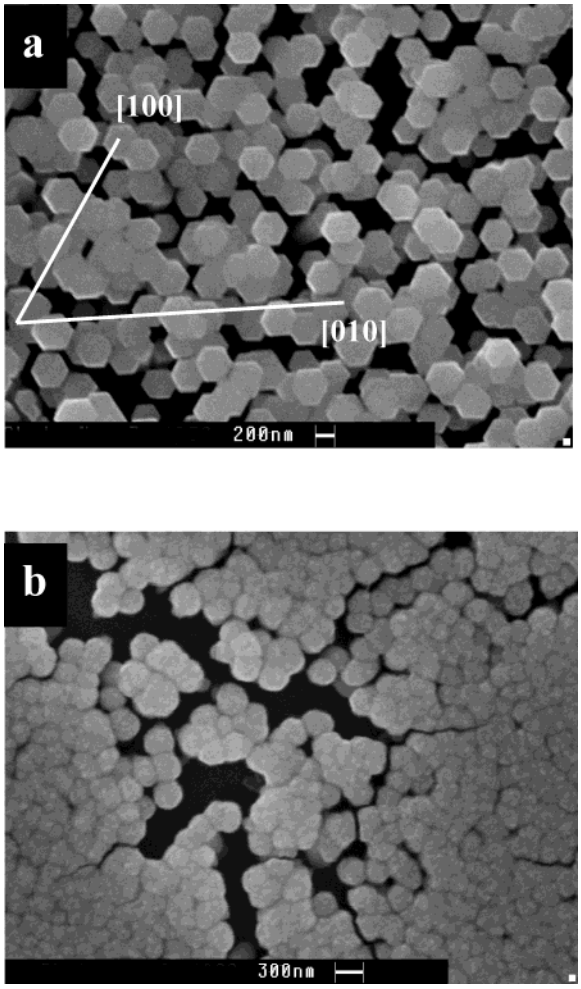

Figure 1. SEM views of hybrid epitaxial films deposited from baths containing 21 μM EY. (a) $E_d = -1.2$ V, $t_d = 3600$ s, 100% O_2; (b) $E_d = -1.5$ V, $t_d = 600$ s, 60% O_2.

3. Results and Discussion

3.1. Influence of the Deposition Potential on Film Properties. The surface morphology of films deposited onto GaN at two different potentials, −1.2 and −1.5 V, imaged by scanning electron microscopy (SEM), are presented in Figure 1. At −1.2 V the deposit is made of an array of crystals with hexagonal shape (Figure 1a). This morphology is similar to that obtained with pure zinc oxide.[15] When the deposition potential is made more negative, by only 200−300 mV, i.e., from −1.2 to −1.4 or −1.5 V, the aspect of the deposit changes dramatically. The hexagonal shape disappears, and the grains appear rounded with no sharp crystalline facets (Figure 1b). This growth mode is thus completely different from that of pure zinc oxide at any potential. The morphological change with the deposition potential is correlated to the change of the redox form of eosin Y during the deposition process. The transition between the oxidized and reduced dye forms (that we shall note o-EY and r-EY, respectively, in the following) in the presence of 5 mM Zn^{2+} in solution is reported at a critical potential, E_c, of ca. −1.3 V.[13] The reaction and the two dye structures are presented in Figure 2.

The variations of the current density during the deposition process, in the absence and in the presence of 21 μM EY, are presented in Figure 3. The comparison between curves a and b shows that $|j_d|$ increases significantly with the presence of dye in solution, even if its concentration is about 25 times lower than that of dissolved oxygen (8×10^{-4} M at saturation),

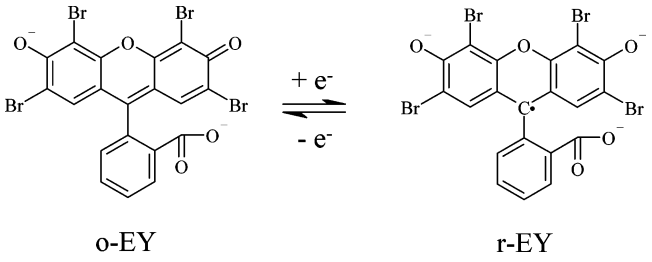

Figure 2. Redox reaction of eosin Y in neutral medium.

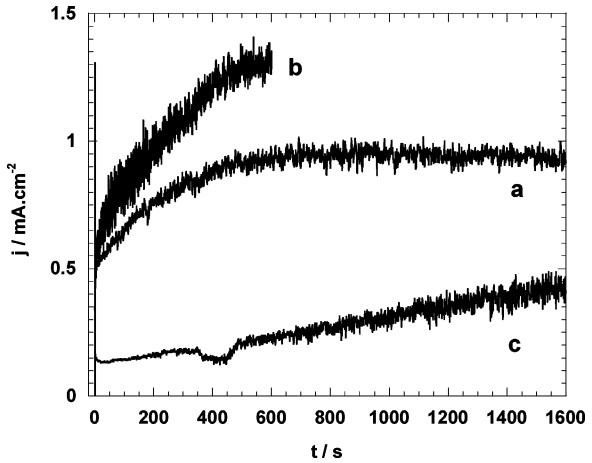

Figure 3. Variation of cathodic current with time: (a) without dye, $E_d = -1.5$ V, 63% O_2; (b) same as (a) with 21 μM EY added; (c) 21 μM EY, $E_d = -1.2$ V, 100% O_2.

TABLE 1: Properties of the Hybrid Films in Relation to the Redox State of EY during Deposition[a]

deposn potential/V vs MSE	redox state of EY	amt of loaded dye/ mol·cm^{-2}	film thickness[b]/μm	dye concn in the film/M
−1.1	o-EY	6.2×10^{-9}	1.1	0.06
−1.4	r- EY	1.4×10^{-7}	5.2	0.26

[a] Nonepitaxial films deposited onto F-doped SnO_2 covered glass substrates from a solution containing 25 μm EY. [b] Measured by profilometry.

which controls the deposition current. We have observed (not shown) that the beneficial effect of EY concentration on the mean current density decreases with the deposition overvoltage. The deposition current density, j_d, increases markedly between −1.2 V (curve c) and −1.5 V (curve b). At −1.2 V, the current density continuously increases with time, whereas at higher overvoltage the main current rise occurs at the beginning of the deposition process.

The film dye loading can be calculated from visible absorption spectroscopy titration after full film dissolution in a known volume of concentrated ammonia solution.[12] This parameter is found dependent on the redox state of EY during the deposition process (Table 1). EY is incorporated at rather high concentration whatever the deposition potential, with a tendency to higher values in the case of r-EY: 0.06 M in films deposited at −1.1 V and 0.26 M in films deposited at −1.4 V when the deposition solution contained 25 μM EY and oxygen was at saturation (Table 1). The presence of eosin in the different deposits is also simply qualitatively evidenced by visual inspection since as-grown films at $E > E_c$ are red colored. Those prepared at $E < E_c$ are transparent during growth but become red after a slow reoxidation process at air contact. After full coloration, the optical transmission curves of epitaxial films revealed the typical absorption peak of o-EY at ca. 520 nm (pointed out by an arrow in Figure 4). In the following, we shall denote these films "r-EY/ZnO", even if the dye is slowly reoxidized by air. The comparison of optical absorption of o-EY/ZnO and r-EY/ZnO films in Figure 4 shows that the height of this peak is higher in the latter case. After thickness correction (the properties of both films are summarized in Table 2), we found results in agreement with dye titration data reported above. The epitaxial films under investigation were rather thin if compared to classical DSSE hybrid films, but it is noteworthy that the maximum absorbance for both films is high. For the sake of comparison, we can mention that an absorbance maximum of 0.26 at 524 nm is reported in the case of a 3 μm N719−ZnO-based DSSE photoanode.[6] The presence of pronounced waves in Figure 4 is due to optical interference fringes. They emphasize the high optical quality of the present epitaxial films.

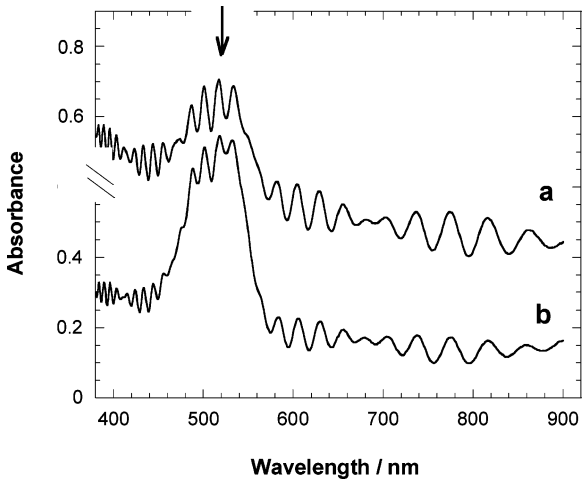

Figure 4. Optical absorbance spectra of hybrid epitaxial films: (a) film presented in Figure 1a, with a theoretical thickness of 1.54 μm; (b) film presented in Figure 1b, with a theoretical thickness of 0.73 μm. (The arrow points out the maximum of o-EY absorbance at $\lambda_{max} = 520$ nm.)

The change of deposit morphology and dye loading with the redox state of EY during deposition is also accompanied by a change of microstructure. This is suggested by dye desorption experiments and photocurrent measurements.[25] The direct observation of the films by transmission electron microscopy gives unambiguous evidence of the key role of EY redox state in film microstructure. In the case of o-EY/ZnO each grain forms an unique and dense single crystal (not shown), as observed in the case of pure ZnO.[17] We can suppose that the dye is occluded in the bulk material and that the structure is closed.

TABLE 2: Deposition Conditions and In-Plane Misorientation of Different Epitaxial Films

sample	film composition	E_d/V vs MSE	[O_2]/mM	j_d[a]/mA·cm^{-2}	theor thickness[b]/μm	dye concn in the film[c]/M	fwhm/deg
a	ZnO	−1.5	0.13	1.3	1.71	0	1.9
b	o-EY/ZnO	−1.2	0.2	0.57	1.54	0.05	3.1
c	r-EY/ZnO	−1.5	0.12	1.63	0.73	0.22	4.0

[a] Mean cathodic current density during deposition. [b] $(M \int_0^{t_d} j_d(t)\, dt)/(2F)$, where t_d is the deposition time, M is the molar volume of ZnO (14.5 cm^3·mol^{-1}), and F is the Faraday constant (96 500 C·mol^{-1}). [c] Calculated from Table 1 and dissolved dye concentration in the deposition bath (21 μM). The loading is assumed in proportion to this latter parameter, as shown in ref 13.

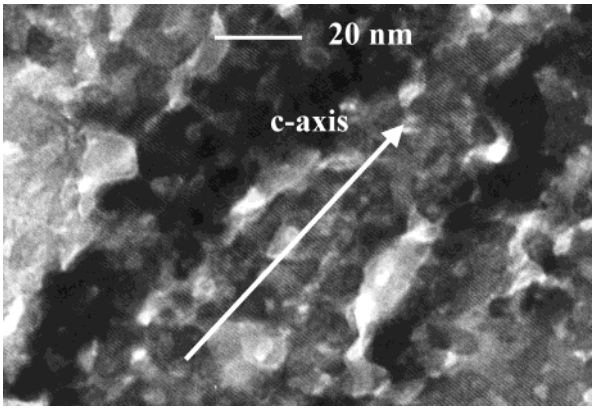

Figure 5. High-resolution TEM cross-sectional view of an r-EY/ZnO crystallite.

The structure of r-EY/ZnO films is dramatically different (Figure 5). We can observe the presence of grains, 5−10 nm in diameter, and also the presence of parallel lines throughout the transmission micrograph. These lines are assigned to the (0001) planes as confirmed by a selected area electron diffraction pattern which shows a spot pattern corresponding to the (0001) family of planes. The stacking of these (0001) planes is very regular. They are parallel to the substrate surface. A conclusion of TEM observations is that the bulk of each crystallite observed in Figure 1b is made of nanograins forming an unique single crystal. TEM also reveals a marked alternate succession of contrasted areas changing from dark to clear in a direction perpendicular to the *c*-axis, suggesting the presence of a mesoporous open network going throughout the crystallites. The diameter of these pores can be estimated at 20 nm. Furthermore, we can suppose that the dye is accumulated in these pores, close

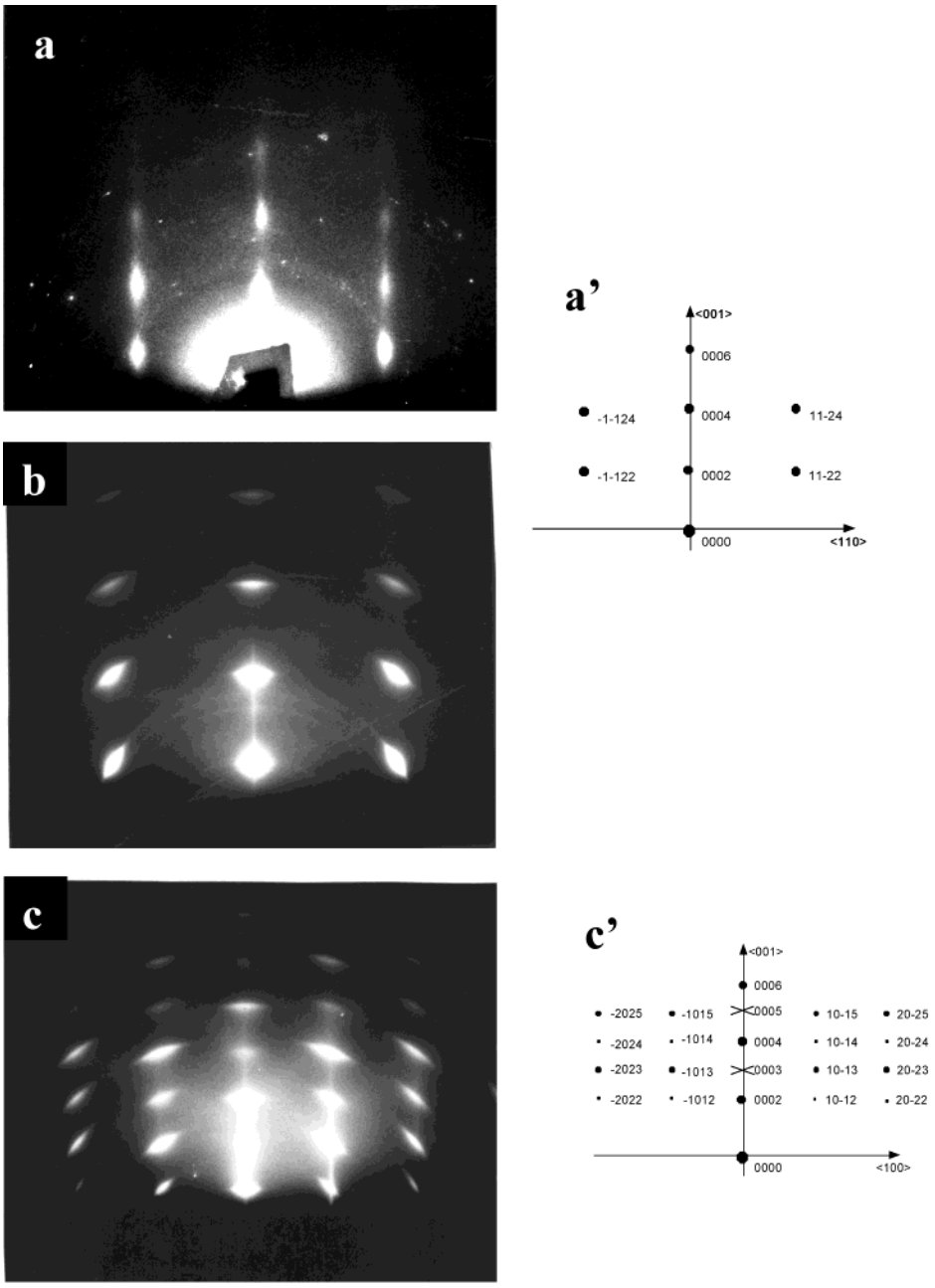

Figure 6. RHEED pattern of (a) the o-EY/ZnO film presented in Figure 1a observed along the ⟨110⟩ azimuth and (a′) indexation diagram of this azimuth with the hexagonal compact structure. (b, c) RHEED pattern of the r-EY/ZnO film presented in Figure 1b: (b) ⟨110⟩ azimuth, (c) ⟨100⟩ azimuth, and (c′) indexation diagram of azimuth in (c) with the hexagonal compact structure.

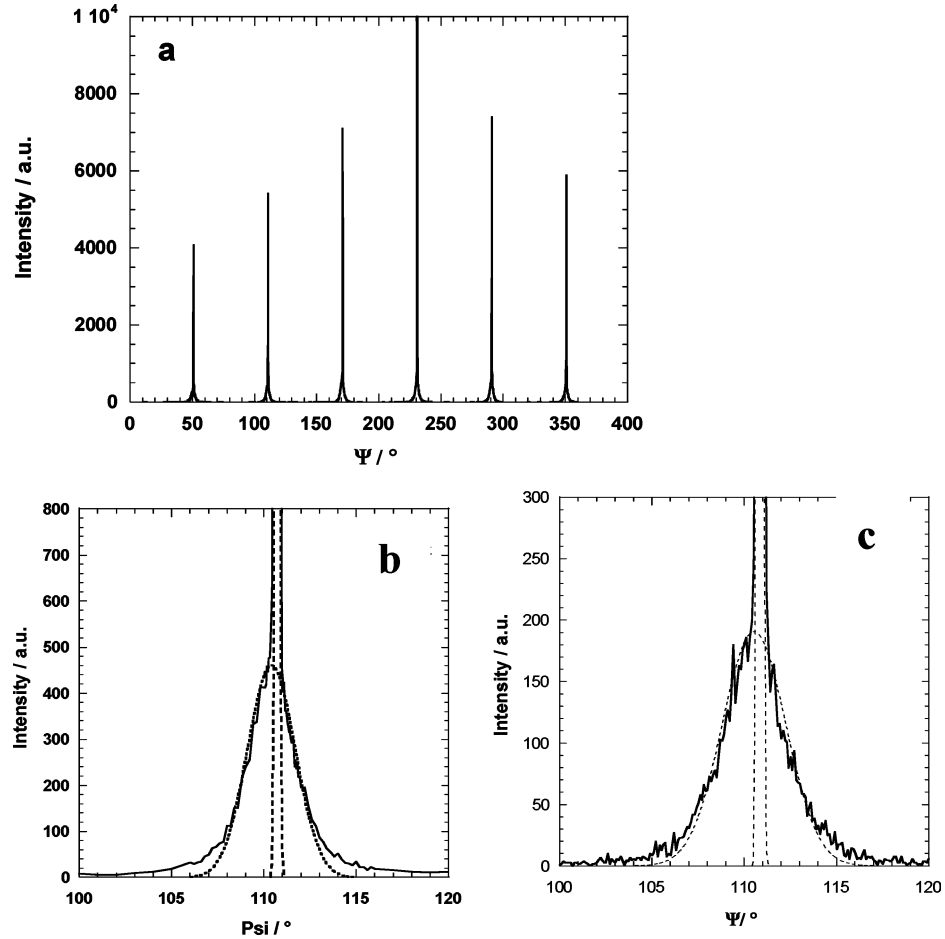

Figure 7. GA-XRD pattern of the $\{10\bar{1}1\}$ lines of the epitaxial (a, b) o-EY/ZnO film deposited at −1.2 V. (a) 360° Ψ-scan; (b) same as (a), enlarged view of an o-EY−ZnO/GaN peak (dotted line, fit of the ZnO contribution; dashed line, fit of the GaN contribution); (c) epitaxial r-EY/ZnO film presented in Figure 1b (pattern and deconvolution curves with the same legend as (b)).

packed and anchored to the zinc oxide matrix surface by means of their carboxyl groups.[35] Eosin, in its reduced redox state, appears to play a key role as a self-organized template for the formation of such a singular structure since it is not observed in the case of oxidized eosin. Further studies are ongoing to better understand the role of the dye in film growth.

3.2. Characterization of the Epitaxial Structure. *3.2.1. o-EY/ZnO Films.* In Figure 1a, the fact that the basic ZnO crystallographic directions, given by the grain edges, are parallel from one grain to the other clearly indicates that the orientation of the o-EY/ZnO deposit is directly related to that of the substrate. This is direct and very elegant evidence of epitaxial growth, as previously demonstrated in the case of pure zinc oxide.[15,17] The epitaxial growth has been confirmed by RHEED experiments, as shown in Figure 6a. The diffraction pattern is observed along the ⟨110⟩ azimuth. It can be indexed with the hexagonal würtzite structure of ZnO (Figure 6a′). The elongation of the spots perpendicular to the horizontal direction shows that the outer surface is smooth.

The in-plane structural relationship between GaN and ZnO has been investigated by glancing-angle X-ray diffraction (GA-XRD). Figure 7a shows a spectrum recorded over a 360° rotation around an axis perpendicular to the substrate (Ψ-scan). For investigating the {101} family of planes, the incident beam was set at 0.6° in order to increase the X-ray path in the film in the order of 100 times. The detector was placed in the Bragg conditions at an height angle of 17.065° versus the sample surface. A very large entrance slit was used for the simultaneous investigation of ZnO and GaN peaks. Six peaks are present. Their full width at half-maximum (fwhm), equal to 0.24°, is similar to that of the bare GaN substrate and is assigned to this compound. When the basis of each peak is enlarged (Figure 7b), a shoulder appears on the left-hand side which is absent on the bare substrate pattern and is assigned to ZnO. The GaN and ZnO peaks have been deconvoluted into a sum of two Gaussian curves. The fact that both peaks appear in very close position indicates that the structural relationship is ZnO-(1000)||GaN(1000). The peak shift between GaN and ZnO, $110.71 - 110.39 = +0.32°$, is in good agreement with the theoretical value of 0.38° deduced from the difference in Bragg angles. An important parameter is the width of the ZnO peak which is directly related to the in-plane misorientation between GaN and ZnO. The average value calculated after deconvolution of the six peaks is 3.1°. We can note the negligible baseline in Figure 7b, which shows the absence of polycrystalline phase and the good quality of the ZnO epitaxial deposit.

3.2.2. r-EY/ZnO Films. RHEED patterns reveal that the compounds deposited at 200−300 mV more negative potentials are also single crystalline epitaxial structures despite their singular rounded shape (Figure 6b,c). Parts b and c of Figure 6 show the patterns obtained along the ⟨110⟩ and ⟨100⟩ azimuths, respectively. They are perfectly indexed by the single crystalline hexagonal structure displayed in parts a′ and c′, respectively, of Figure 6. The forbidden reflections (0003) and (0005) are visible in Figure 6c. Compared to what was observed at lower deposition potentials, one can note that the dots tend to be more elongated in the direction perpendicular to ⟨001⟩. This reveals that the in-plane misorientation (mosaicity) is slightly larger in

the present case and can be estimated at a few degrees. The in-plane orientation of the deposit remains the same as that of the substrate but with some angular deviations from one grain to the other.

This point has been confirmed by GA-XRD Ψ-scan experiments. The general pattern is similar to that found at lower overvoltage (not shown). As in the previous case, an enlarged bottom of the GaN peaks is observed during a Ψ-scan. Figure 7c shows an enlarged view of one of them and the two Gaussian fitting curves resulting in its deconvolution. The fwhm of the ZnO Gaussian fit is enlarged compared to Figure 7b, with a mean value of 4.0°. The quantity of polycrystalline ZnO remains negligible. The different films studied were quite thick (calculated at 0.7−1.5 μm thick assuming a deposition efficiency of 1 and a density of 5.6 g·cm^{-3}). Therefore, the epitaxy is not lost during the growth and no critical thickness is found. That means that, even for high dye loading, the growth of ZnO continues in a homoepitaxial manner and there is no thickness limit above which the epitaxy would be lost.

Table 2 compares the in-plane misorentations of an epitaxial pure ZnO film deposited at −1.5 V and of the two different kind of hybrid deposits defined above. The deposition conditions are also summarized. According to these data, we can conclude that the decrease of the in-plane matching in the presence of EY is not due to a rise of the deposition rate (compare samples a and c) and is neither due to film thickness (compare samples a and c). The detrimental parameter seems to be the dye loading: the higher the dye concentration in the film, the higher the fwhm. This can be explained by a partial inhibition of the ZnO structural unit matching with the GaN surface following the dye anchoring on ZnO by means of the carboxyl group.

In summary, we have shown for the first time that an organic/inorganic hybrid film can be electrodeposited in one step in an epitaxial manner. The investigated system was EY/ZnO on GaN-(0001) substrate. The dye loading is high, with upper values in the 0.2−0.3 M range. The in-plane epitaxial relationship is ZnO-(1000)||GaN(1000). The epitaxy is maintained over the deposition potential range of the hybrid films (between −1.2 and −1.5 V) even if the morphology changes dramatically between the films deposited in the presence of oxidized EY and reduced EY with a transition between hexagonal rods and round crystallites. The films present a good in-plane orientation and a negligible amount of polycrystalline ZnO. The in-plane misorientation of the layer is increased with the presence of dye in the film, and the poorest in-plane matching with r-EY compared to o-EY is explained by a higher dye loading. The presence of dye in the film, bonded to ZnO, impinges to some extent the in-plane matching without completely inhibiting the epitaxial growth. In hexagonal-shaped hybrid crystallites, the dye is occluded in the bulk material, and the structure is closed, whereas an open structure, highly loaded by the dye, is found when the zinc oxide is coprecipitated with EY in a reduced state. These latter films behave as promising sensitized photoanodes.[25] The role of the redox state of EY on the deposition mechanism and hybrid microstructure is under investigation and will be discussed in more detail in a forthcoming communication.

Acknowledgment. The authors are very grateful to Dr. Bernard Baumont (Centre de Recherche sur l'Hétéroépitaxie et ses Applications, Sophia Antipolis, France) for supplying them with GaN single crystals. Stephan Borensztajn (UPR15, Paris) is acknowledged for the SEM observation of the samples.

References and Notes

(1) Sanchez, C.; de A. A. Soler-Illia, G. J.; Ribot, F.; Lalot, T.; Mayer, C. R.; Cabuil, V. *Chem. Mater.* **2001**, *13*, 3061.
(2) Sanchez, C.; Ribot, F.; Lebeau, B. *J. Mater. Chem.* **1999**, *9*, 35.
(3) Ogawa, K.; Kuroda, K. *Chem. Rev.* **1995**, *95*, 399.
(4) Coronado, E.; Mingotaud, C. *Adv. Mater.* **1999**, *11*, 869.
(5) O'Reagan, B.; Grätzel, M. *Nature* **1991**, *353*, 737.
(6) Shklover, V.; Ovchinnitov, Y. E.; Braginsky, L. S.; Zakeeruddin, S. M.; Grätzel, M. *Chem. Mater.* **1998**, *10*, 2533.
(7) Cahen, D.; Hodes, G.; Grätzel, M.; Guillemoles, J. F.; Riess, I. *J. Phys. Chem. B* **2000**, *6*, 686.
(8) Bauer, C.; Boschloo, G.; Mukhtar, E.; Hagfeldt, A. *J. Phys. Chem. B* **2001**, *105*, 5585.
(9) Yoshida, T.; Tochimoto, M.; Schlettwein, D.; Wöhrle, D.; Sugiura, T.; Minoura, H. *Chem. Mater.* **1999**, *11*, 2657.
(10) Yoshida, T.; Minoura, H. *Adv. Mater.* **2000**, *12*, 1219.
(11) Okabe, K.; Yoshida, T.; Sugiura, T.; Minoura, H. *Trans. Mater. Res. Soc. Jpn.* **2001**, *26*, 523.
(12) Yoshida, T.; Terada, K.; Schlettwein, D.; Oekermann, T.; Sugiura, T.; Minoura, H. *Adv. Mater.* **2000**, *12*, 1214.
(13) Pauporté, T.; Yoshida, T.; Goux, A.; Lincot, D. *J. Electroanal. Chem.* **2002**, *534*, 55.
(14) Kuruppuchamy, S.; Yoshida, T.; Sugiura, T.; Minoura, H. *Thin Solid Films* **2001**, *397*, 63.
(15) Pauporté, T.; Lincot, D. *Appl. Phys. Lett.* **1999**, *75*, 3817.
(16) Liu, R.; Vertegel, A. A.; Bohannan, E. W.; Sorenson, T. A.; Switzer, J. A. *Chem. Mater.* **2001**, *13*, 508.
(17) Pauporté, T.; Cortès, R.; Froment, M.; Beaumont, B.; Lincot, D. *Chem. Mater.* **2002**, *14*, 4702.
(18) Peulon, S.; Lincot, D. *Adv. Mater.* **1996**, *8*, 166.
(19) Pauporté, T.; Lincot, D. *Electrochim. Acta* **2000**, *45*, 3345.
(20) Izaki, M.; Omi, T. *Appl. Phys. Lett.* **1996**, *68*, 2439.
(21) Pauporté, T.; Lincot, D. *J. Electrochem. Soc.* **2001**, *148*, C310.
(22) Pauporté, T.; Lincot, D. *J. Electroanal. Chem.* **2001**, *517*, 54.
(23) Madelung, O. *Semiconductors—Basic Data*; Springer: Berlin, 1996.
(24) Froment, M.; Bernard, M. C.; Cortes, R.; Mokili, B.; Lincot, D. *J. Electrochem. Soc.* **1995**, *142*, 2642.
(25) Yoshida, T.; Pauporté, T.; Lincot, D.; Oekermann, T.; Minoura, H. *J. Electrochem. Soc.* **2003**, *150*, C608.